Chinese Chemical Letters 35 (2024) 110014

Contents lists available at ScienceDirect

Chinese Chemical Letters

journal homepage: www.elsevier.com/locate/cclet

# Additive regulating $Li^+$ solvation structure to construct dual LiF–rich electrode electrolyte interphases for sustaining 4.6 V Li||$LiCoO_2$ batteries

Xi Tang[a], Chunlei Zhu[a], Yulu Yang[a], Shihan Qi[a], Mengqiu Cai[a], Abdullah N. Alodhayb[b], Jianmin Ma[a,*]

[a] School of Physics and Electronics, Hunan University, Changsha 410082, China
[b] Department of Physics and Astronomy, College of Science, King Saud University, Riyadh 11451, Saudi Arabia

ARTICLE INFO

*Article history:*
Received 29 June 2023
Revised 8 April 2024
Accepted 14 May 2024
Available online 11 September 2024

*Keywords:*
Lithium metal batteries
Electrolyte additive
Solid electrolyte interphase
Cathode electrolyte interphase
Solvation structure

ABSTRACT

The battery energy density can be improved by raising the operating voltage, however, which may lead to rapid capacity decay due to the continuous electrolyte decomposition and the thickening of electrode electrolyte interphases. To address these challenges, we proposed tripropyl phosphate (TPP) as an additive–regulating $Li^+$ solvation structure to construct a stable LiF–rich electrode carbonate–based electrolyte interphases for sustaining 4.6 V Li||$LiCoO_2$ batteries. This optimized interphases could help reduce the resistance and achieve better rate performance and cycling stability. As expected, the Li||$LiCoO_2$ battery retained 79.4% capacity after 100 cycles at 0.5 C, while the Li||Li symmetric cell also kept a stable plating/stripping process over 450 h at the current density of 1.0 mA/$cm^2$ with a deposited amount of 0.5 mAh/$cm^2$.



As one of typic commercial cathode materials, $LiCoO_2$ has huge potential as high–capacity cathode for lithium metal batteries (LMBs) [1–3], especially coupled with Li anode [4–6], since only half of the theoretical capacity of $LiCoO_2$ can be delivered at the cut–off voltage of 4.25 V. Thus, the energy density of Li||$LiCoO_2$ batteries can be promoted by raising the cut–off voltage [7–10]. Unfortunately, traditional carbonates have strong binding ability with $Li^+$ that are difficult to desolvation, which leads to slow reaction kinetics. Moreover, the strong coordination of EC and EMC with $Li^+$ lead to serious side reactions with $LiCoO_2$, resulting in loose porous organic cathode electrolyte interphase (CEI), which is constantly broken/reconstructed during the charge/discharge process, resulting in continuous consumption of electrolyte and rapid capacity decay [11–13]. Moreover, the continuous accumulation of non–conducting and fragile solid electrolyte interphase (SEI) leads to poor interface stability and uncontrolled growth of Li dendrites, which reduce the capacity and coulomb efficiency (CE) [14–19]. Therefore, it is very crucial to promote cycling stability and rate capability by optimizing CEI and SEI in high–voltage Li||$LiCoO_2$ batteries [20–23].

Electrolyte additive strategy is demonstated to effectively improve CEI/SEI performance [24–28]. Among them, phosphates are well–known co–solvents and additives due to their non–flammability and film–forming properties [29–31]. Moreover, phosphate–based additives are also reported to improve the cycling performance of lithium–ion batteries at elevated temperatures by constructing superior electrode electrolyte interphases [32]. However, the efficient phosphate–based additives are rarely reported in high–voltage Li||$LiCoO_2$ batteries.

In this work, we proposed an additive regulating $Li^+$ solvation structure strategy for constructing dual LiF–rich electrode electrolyte interphases to support 4.6 V Li||$LiCoO_2$ batteries. For the cathode, the well–formed CEI with inorganic substances restrains the harassing oxidative decomposition of solvents. For the anode, TPP promotes the formation of SEI enriched in fluoride/phosphide components, which facilitates uniform Li deposition and suppresses the formation of Li dendrites [33,34]. This work contributes to a deep comprehensive understanding of the specific working mechanism of phosphate additives.

To investigate the electrochemical stability and solvation effects of the phosphate–based additives, the theoretical prediction based on density functional theory (DFT) and molecular dynamics (MD) simulations were carried out (Fig. 1). Among the molecules, EMC and TPP have the highest HOMO and are easily oxidized while FEC

* Corresponding author.
*E-mail address:* nanoelechem@hnu.edu.cn (J. Ma).

https://doi.org/10.1016/j.cclet.2024.110014
1001-8417/

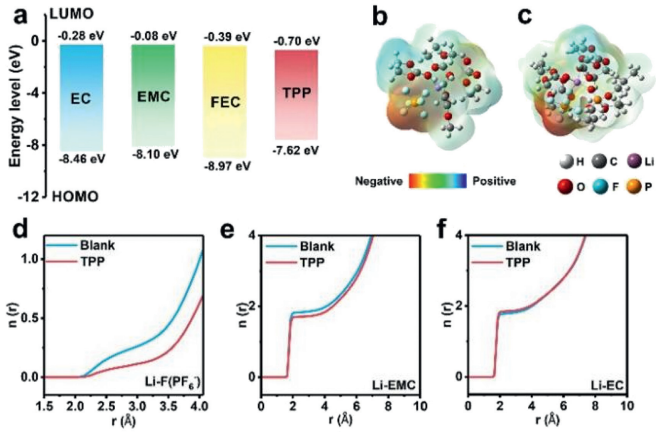


**Fig. 1.** Theoretical prediction of phosphate−based additives. (a) LUMO (lowest unoccupied molecular orbital) and HOMO (highest occupied molecular orbital) energy values of carbonate solvent molecules and TPP. Schematic diagrams of the ESP charge distribution in the solvated sheath of (b) blank electrolyte and (c) TPP−contained electrolyte. Molecular dynamics simulation of $Li^+$ in different electrolytes, the cumulative coordination number ($n$(r)) of $Li^+$ with (d) $PF_6^-$ anion, (e) FEC molecule, and (f) EC molecule.

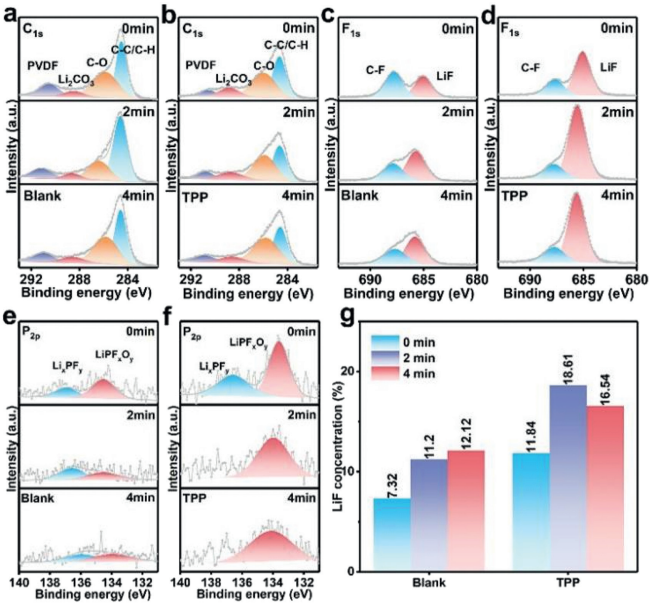


**Fig. 2.** XPS curves of CEI on LCO cathode, formed in different electrolyte systems. C 1s spectra: (a) Blank electrolyte and (b) TPP−contained electrolyte. F 1s spectra: (c) Blank electrolyte and (d) TPP-contained electrolyte. P 2p spectra: (e) Blank electrolyte and (f) TPP-contained electrolyte. (g) Content of LiF of the CEI of blank and TPP−contained electrolytes.

and TPP exhibit the lowest LUMO and are easily reduced (Fig. 1a), which provides a thermodynamic basis for the growth of interphases. The MD simulation results in Figs. 1b-f show that the $Li^+$ in the blank electrolyte is closely coordinated with EC and EMC, which are carried to the electrode surface for oxidation to form various loose and unstable organic by−products. As expected, the highly electronegative O atom of TPP coordinates with $Li^+$ and occupies the solvated group, reducing the coordination number of anions and solvent molecules due to its large steric hindrance (Fig. S1 in Supporting information). Therefore, in the process of charging, more free $PF_6^-$ are preferentially adsorbed on the surface of the positively charged $LiCoO_2$ under electrostatic action than the $Li^+$−solvent complexes, realizing the anion−dominated inner Helmholtz plane (IHP) and the formation of inorganic species−rich CEI layer. At the same time, the solvation degree of weakly coordinated FEC increases with the influence of TPP, which is conducive to the formation of LiF−rich SEI.

To build a deeper understanding of the phosphate−based additive, the surface chemical compositions of CEI films formed in different electrolytes were characterized by X−ray photoelectron spectroscopy (XPS). As shown in Fig. 2, Figs. S2 and S3 (Supporting information), the depth profile of the $LiCoO_2$ electrode was detected by Ar sputtering at 2 min and 4 min. The CEI films in all electrolytes contain organic components (C−F, C−O, C=O and C−C/C−H) and inorganic components ($Li_2CO_3$, LiF and $LiPF_xO_y$). The C signal peaks in Figs. 2a and b and Fig. S3 show that the organic compounds (C−O, C−C peaks) from the decomposition of carbonate solvents are abundant in the CEI formed in the blank electrolyte, suggesting a large amount of electrolyte consumption during the cycling process. The organic−rich CEI is quite tightly bound to the $LiCoO_2$ surface and cannot withstand the large volume changes generated by the oxide cathode during the cycling process, resulting in CEI fragmentation and continuous side reactions between the $LiCoO_2$ and electrolyte during the lithiation/delithiation process [35,36]. In sharp contrast, the anions are well adsorbed in the IHP of $LiCoO_2$ with the attraction of electrostatic field due to the exisitence of TPP, and then decomposed into the LiF−rich CEI. The bonding energy of the inorganic substances and transition metal oxide is relatively weak, which can accommodate the repeating volume change during cycling and play a positive role in protecting the cathode material [37]. In addition, the decomposition product LiF of $PF_6^-$ has a wide electrochemical stability window, which passivates $LiCoO_2$ surface [38]. The LiF−rich CEI effectively hinders the interface side reactions between the highly oxidized $LiCoO_2$ and the electrolyte, and reduces solvent molecular consumption. As can be seen from Figs. 2c−g, the strong signals of LiF and $LiPF_xO_y$ in the inner layer of CEI with TPP indicate the formation of anion−derived CEI, which is consistent with the speculation. In addition, due to the highest HOMO, a trace amount of TPP can be also decomposed on $LiCoO_2$ to provide phosphide components for CEI.

To visually assess the enhancement effect of TPP on $LiCoO_2$ cathode, Li||$LiCoO_2$ batteries with different electrolytes were measured in a voltage range of 3−4.6 V. As shown in Fig. 3a, the battery with TPP shows a little higher initial discharge capacity of 187.7 mAh/g while the capacity remained at 149.0 mAh/g with a retention rate of 79.4% after 100 cycles. By contrast, the battery without TPP only shows a low retention rate of 67.9% over 100 cycles. The voltage polarization can be demonstrated by the voltage profile curve visually. As shown in Fig. 3b, the capacity of the battery with blank electrolyte decreases and the polarization voltage increases rapidly over 100 cycles, which is attributed to the intense side reactions between the electrolyte and $LiCoO_2$ as well as the continuous fragmentation/remodeling of CEI. However, the polarization voltage of the battery with TPP has little change (Fig. 3c). In Fig. 3d, the impedance of the battery with TPP is significantly lower than that of the battery with blank electrolyte since the almost same battery impedances before cycling (Fig. S4 in Supporting information). Moreover, the equivalent circuits and fitting results of the EIS were shown in Fig. S5 (Supporting information), which exhibits a much smaller charge transfer impedance ($R_{ct}$) of the battery with TPP than that with blank electrolyte after 10 cycles. The EIS results revealed the fast electrochemical reaction kinetics in the electrolyte with TPP. Furthermore, the transmission electron microscopy (TEM) characterizations visually display the explicit shape of CEI (Figs. 3e and f). Due to the extremely low electronic conductivity of LiF, the anion−induced CEI with TPP is thin and compact, while the CEI with blank electrolyte is bumpy. The firm CEI structure with TPP provides the sustainable basis of

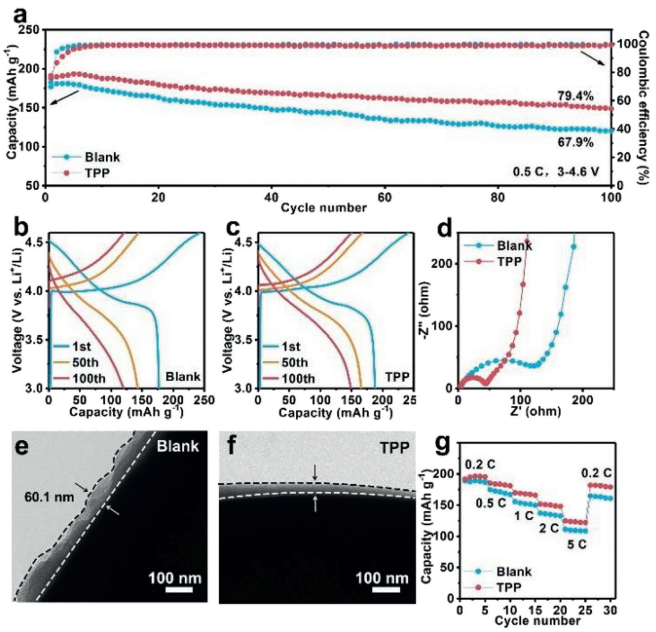


**Fig. 3.** Electrochemical performances of Li||LCO cell assembled with different electrolyte systems: (a) Cycling performances. (b) Charge–discharge profiles of blank electrolyte and (c) TPP contained electrolyte. (d) EIS profiles after 10 cycles. (e, f) TEM images of CEI on the cathode and (g) rate performances, test in a voltage range of 3–4.6 V (*vs.* $Li^+$/Li).

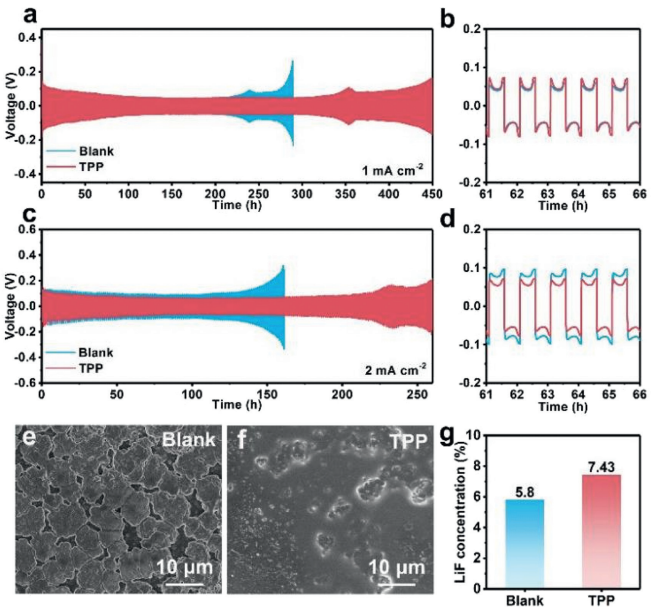


**Fig. 4.** Li dendrite inhibition effect of TPP. (a) Li plating/stripping cycling performance and (b) magnified time–voltage profiles during selected cycle time, under 1.0 mA/cm$^2$, 0.5 mAh/cm$^2$. (c) Li plating/stripping cycling performance and (d) magnified time–voltage profiles during selected cycle time, under 2.0 mA/cm$^2$, 1.0 mAh/cm$^2$. SEM images of cycled lithium metal anode in different electrolyte systems (after 25 cycles): (e) Blank electrolyte, (f) TPP–contained electrolyte. (g) Content of LiF on anode surface with blank and TPP–contained electrolytes after 10 cycles.

the repeated lithiation/delithiation. Furthermore, the battery with TPP exhibits enhanced rate capacities of 194.9, 180.3, 168.1, 149.9, 123.3 mAh/g at current densities of 0.2, 0.5, 1, 2, and 5 C, respectively, and returns to 189.2 mAh/cm$^2$ at 0.2 C (Fig. 3g), while a capacity of 109.7 mAh/g is delivered at 5 C for battery with blank electrolyte, which indicates the formation of fast $Li^+$ transport dynamics in the CEI formed with TPP.

Finally, the phosphate−based additive also has an impact on Li plating/stripping. As shown in Figs. 4a and b, the Li||Li symmetric cell with TPP could maintain a stable plating/stripping process over 450 h at the current density of 1.0 mA/cm$^2$ with the capacity of 0.5 mAh/cm$^2$ while only 285 h is sustained for the cell with blank electrolyte. At lower current density, the cells with/without TPP exhibit the same polarization voltage value. The cell with TPP exhibits the longer plating/stripping process in ∼260 h with a lower polarization voltage when the current density increases to 2.0 mA/cm$^2$ (Figs. 4c and d). As shown in Figs. 4e and f, Li deposited into a bulb shape in the blank electrolyte. The transport of $Li^+$ was hindered by the accumulated layer of dead Li. In contrast, the plated Li anode with TPP exposed a smooth surface without projecting Li dendrites. The bulk Li with dense and overlapping surface maintains structural integrity during the plating/stripping process, avoiding battery safety issues caused by Li dendrites piercing the diaphragm. The surface morphologies of the Li anodes correspond to the performances of the symmetrical cells [39]. The SEI formed on the Li anodes were further characterized by XPS, which are composed of organic/inorganic components including C−C/C−H, C−O/C=O, $ROCO_2Li$, $Li_2CO_3$, LiF and $LiPF_xO_y$. The results are shown in Fig. 4g and Figs. S6−S8 (Supporting information). According to the $Li^+$ solvation results, the most easily reducible FEC with low LUMO in the solvation group is enhanced, and the TPP is involved in solvation and decomposed on Li surface, which provides high F and P content for SEI, respectively. Thus, the SEI formed with TPP contains rich LiF produced by the decomposition of FEC, which is a strong electrical insulator for suppressing the continuous consumption of the electrolyte by resisting the electrons that passing through the SEI layer [40,41]. Besides, LiF exhibits lithiophobicity properties and high Young's modulus, which can promote the lateral growth and the uniform deposition of new Li on the anode surface [42]. Moreover, $LiPF_xO_y$ provides the SEI with high ionic conductivity and reduced impedance, which enables efficient transport of $Li^+$ and allows the battery to exhibit better rate performance [43].

In summary, we have successfully explored a phosphate−contained high−voltage electrolyte for 4.6 V Li||$LiCoO_2$ batteries. TPP could regulate the $Li^+$ solvation structure to optimize the structure and components of CEI/SEI. The designed anion−derived CEI with plenty LiF component forms a parclose to protect the $LiCoO_2$ structure and reduce the persistent side reactions of solvents. At the same time, the TPP−induced SEI with high content of F and P radicals guarantees excellent anode stability. This work demonstrate the effectiveness of electrolyte additives to optimize the structure and components of electrode electrolyte interphases *via* regulating the $Li^+$ solvation structure.

## Declaration of competing interest

We herein declare that there is not any conflict in this manuscript.

## CRediT authorship contribution statement

**Xi Tang:** Writing – original draft. **Chunlei Zhu:** Visualization. **Yulu Yang:** Formal analysis. **Shihan Qi:** Formal analysis. **Mengqiu Cai:** Writing – review & editing. **Abdullah N. Alodhayb:** Writing – review & editing. **Jianmin Ma:** Writing – review & editing.

## Acknowledgments

The project was supported by the National Natural Science Foundation of China (No. U21A20311) and the Distinguished Sci-

entist Fellowship Program (DSFP) at King Saud University, Riyadh, Saudi Arabia.

## Supplementary materials

Supplementary material associated with this article can be found, in the online version, at doi:10.1016/j.cclet.2024.110014.

## References

[1] J.C. Zhang, Z.D. Liu, C.H. Zeng, et al., Rare Met. 41 (2022) 3946–3956.
[2] D. Li, B. Zhang, X. Ou, et al., Chin. Chem. Lett. 32 (2021) 2333–2337.
[3] Q. Wu, B. Zhang, Y. Lu, J. Energy Chem. 74 (2022) 283–308.
[4] Y. Wang, Q. Zhang, Z.C. Xue, et al., Adv. Energy Mater. 10 (2020) 2001413.
[5] J. Huang, Y. Zhu, Y. Feng, et al., Acta Phys. Chim. Sin. 38 (2022) 2208008.
[6] X. Chen, Q. Sun, J. Xie, et al., J. Energy Chem. 74 (2022) 91–99.
[7] G.G. Bizuneh, C. Zhu, J. Huang, et al., Small Methods 7 (2023) 2300079.
[8] J. Liu, M. Wu, X. Li, et al., Adv. Energy Mater. 13 (2023) 2300084.
[9] K. Guo, C. Zhu, H. Wang, et al., Adv. Energy Mater. 13 (2023) 2204272.
[10] F. Xian, J. Li, Z. Hu, et al., Chem. Commun. 56 (2020) 4998–5001.
[11] J. Zhang, H. Zhang, S. Weng, et al., Nat. Commun. 14 (2023) 2211.
[12] Z. Sun, H. Zhou, X. Luo, et al., J. Power Sources 503 (2021) 230033.
[13] Y. Lyu, X. Wu, K. Wang, et al., Adv. Energy Mater. 11 (2021) 2000982.
[14] X. Hu, J. Liu, Y. Yang, et al., Chin. Chem. Lett. 34 (2023) 108456.
[15] R. Yu, Z. Li, X. Zhang, X. Guo, Chem. Commun. 58 (2022) 8994–8997.
[16] H. Wang, J. He, J. Liu, et al., Adv. Funct. Mater. 31 (2021) 2002578.
[17] S. Qi, J. He, J. Liu, et al., Adv. Funct. Mater. 31 (2021) 2009013.
[18] B. Roy, P. Cherepanov, C. Nguyen, et al., Adv. Energy Mater. 11 (2021) 2101422.
[19] F. Li, J. He, J. Liu, et al., Angew. Chem. Int. Ed. 60 (2021) 6600–6608.
[20] W. Xue, R. Gao, Z. Shi, et al., Energy Environ. Sci. 14 (2021) 6030–6040.
[21] W. Lu, J. Zhang, J. Xu, X. Wu, L. Chen, ACS Appl. Mater. Interfaces 9 (2017) 19313–19318.
[22] K. Zhang, J. Chen, W. Feng, et al., J. Power Sources 553 (2023) 232311.
[23] H. Zhang, Z. Zeng, S. Wang, et al., Nano Res. 17 (2024) 2638–2645.
[24] S. Tan, Z. Shadike, J. Li, et al., Nat. Energy 7 (2022) 484–494.
[25] Z. Guo, H. Yang, Q. Wei, et al., Chin. Chem. Lett. 34 (2023) 108622.
[26] X. Yang, M. Lin, G. Zheng, et al., Adv. Funct. Mater. 30 (2020) 2004664.
[27] Z. Qin, B. Hong, B. Duan, et al., Electrochim. Acta 276 (2018) 412–416.
[28] Y. Sun, J. Huang, H. Xiang, et al., J. Mater. Sci. Technol. 55 (2020) 198–202.
[29] P. Shi, H. Zheng, X. Liang, et al., Chem. Commun. 54 (2018) 4453–4456.
[30] G. Jiang, J. Liu, Z. Wang, J. Ma, Adv. Funct. Mater. 33 (2023) 2300629.
[31] T. Zheng, B. Zhu, J. Xiong, et al., Energy Stor. Mater. 59 (2023) 102782.
[32] H. Zhao, Y. Qian, S. Hu, et al., ACS Appl. Mater. Interfaces 13 (2021) 29676–29690.
[33] J. Tan, J. Matz, P. Dong, J. Shen, M. Ye, Adv. Energy Mater. 11 (2021) 2100046.
[34] D. Wu, J. He, J. Liu, et al., Adv. Energy Mater. 12 (2022) 2200337.
[35] C. Yang, X. Liao, X. Zhou, et al., Adv. Mater. 35 (2023) 2210966.
[36] R. Qi, M. Yang, T. Zheng, et al., Small 20 (2024) 2312087.
[37] J. Liu, B. Yuan, N. He, et al., Energy Environ. Sci. 16 (2023) 1024–1034.
[38] P. Bai, X. Ji, J. Zhang, et al., Angew. Chem. Int. Ed. 61 (2022) e202202731.
[39] Q.K. Zhang, X.Q. Zhang, J. Wan, et al., Nat. Energy 8 (2023) 725–735.
[40] X.Q. Zhang, X.B. Cheng, X. Chen, C. Yan, Q. Zhang, Adv. Funct. Mater. 27 (2017) 1605989.
[41] M.Y. Zhou, X.Q. Ding, J.F. Ding, et al., Joule 6 (2022) 2122–2137.
[42] S. Liu, J. Xia, W. Zhang, et al., Angew. Chem. Int. Ed. 61 (2022) e202210522.
[43] H. Su, Z. Chen, M. Li, et al., Adv. Mater. 35 (2023) 2301171.